In Situ Identification of Surface Sites in Cu-Pt Bimetallic Catalysts: Gas-Induced Metal Segregation*

Tongxin Han, ¹ Yuanyuan Li, ^{2,&} Yueqiang Cao, ³ Ilkeun Lee, ¹ Xinggui Zhou, ³ Anatoly I. Frenkel, ^{2,4} and Francisco Zaera ^{1,*}

¹ Department of Chemistry and UCR Center for Catalysis, University of California, Riverside, CA 92521, USA.

² Department of Materials Science and Chemical Engineering, Stony Brook University, Stony Brook, NY 11794, USA.

³ State Key Laboratory of Chemical Engineering, School of Chemical Engineering, East China University of Science and Technology, Shanghai 200237, China.

⁴ Chemistry Division, Brookhaven National Laboratory, Upton, NY 11973, USA.

[&] Present address: Chemical Sciences Division, Oak Ridge National Laboratory, Oak Ridge, TN 37831, USA.

^{*} Corresponding Author, Email: zaera@ucr.edu

Abstract

The effect of the presence of a gaseous atmosphere on the surface composition of Cu-Pt bimetallic catalysts has been tested by in situ infrared (IR) and X-ray absorption (XAS) spectroscopies. Diffusion of Pt atoms within the Cu-Pt nanoparticles (NPs) was observed both in vacuum and under gaseous atmospheres. Vacuum IR spectra for CO adsorbed on Cu_{1-x}Pt_x/SBA-15 catalysts (x = 0 to 1) at 125 K show no bonding on Pt regardless of Pt content, but some Pt segregation to the surface is seen with the high-Pt-content ($x \ge 0.2$) samples upon heating to 225 K. This behavior was shown to be reversible. *In situ* IR spectra in the presence of atmospheric pressures of CO also highlighted the reversible segregation of Pt to the surface and its diffusion back to the bulk when cycling the temperature from 295 K to 495 K and back. This is the most evident for diluted single-atom alloy (SAA) catalysts, for $x \le 0.01$, but was also seen with more Pt-rich catalysts, albeit following a more complex behavior that depends on both CO pressure and temperature. Similar behavior is also likely to occur under H₂ atmospheres, but this conclusion is tentative due to the possible interference of the CO probe molecule used in those in situ IR experiments. In situ XAS experiments expanded and added to the picture developed using the IR data. The near-edge region of the XAS spectra obtained under both CO and He atmospheres points to the metallic and well-mixed nature of the Pt atoms irrespective of gas or temperature, but analysis of the extended X-ray absorption fine structure (EXAFS) in the sample clearly identifies a change in coordination environment around the Pt atoms, from high fractions of Pt-Pt bonds (coordination to Cu vs. Pt atoms ~ 6:6) at or below 445 K to better dispersion (8:4) at 495 K. The main conclusion is that Cu-Pt bimetallic catalysts are dynamic, with the

composition of their surfaces being dependent on temperature, in particular in gaseous environments.

1. Introduction

Much heterogeneous catalysis, including most hydrogenations of organic feedstocks, relies on the use of late transition metals.¹⁻³ Pt, Pd, and Rh in particular are quite active, and are used extensively for a variety of industrial processes. Unfortunately, late transition metals are not very selective and tend to hydrogenate most if not all of the double and triple bonds in organic molecules with multiple unsaturations. To add flexibility to the design of selective metal-based catalysts, two or more metals can be mixed to create alloys. Bi- and multi-metallic catalysts have in fact been used extensively in catalysis for decades;⁴⁻⁶ mixed metals may display unique electronic properties, often (but not always) a weighted average of the electronic properties of the individual components,⁷⁻¹⁰ and/or mixed-metal ensembles of atoms on the surface with unique catalytic properties ¹¹⁻¹³.

A new version of alloying in catalysis has gained attention in recent years where a majority metal is mixed with small amounts of a second component to create so-called single-atom alloys (SAAs).¹⁴⁻¹⁷ The difference with other more traditional bimetallic catalysts is that, in SAA, the minority component is believed to be present on the surface of the nanoparticles (NPs) in isolated form, far from other atoms of the same metal. The premise guiding the design of SAA catalysts is that the single-atom sites add specific functionality lacking in the majority component, which otherwise is assumed to selectively promote process of interest.^{17, 18} In the case of hydrogenation catalysis, for instance, the addition of small amounts of an active metal such as Pt or Pd may help with the activation of molecular hydrogen, something for which coinage metals such as Cu or Au are not effective;¹⁹⁻²¹ this way, it may be possible to exploit the

presumed selectivity of those coinage metals during the promotion of the hydrogenation steps. 16, 17, 22-25

Empirically, it has become clear that SAA catalysts can in many instances improve the selectivity of hydrogenation reactions. How that occurs, however, is still being debated. Much elegant surface-science work using model metal surfaces such as single crystals and controlled ultra-high vacuum (UHV) environments has been performed 27, 32-34 and complemented with quantum mechanics calculations 35-37 to support a proposed mechanism by which H2 molecules are dissociated on individual Pt or Pd atoms present on the surface, after which the resulting adsorbed H atoms spill over to the Cu or Au surfaces where the organic molecules are hydrogenated. However, more recent evidence from our group and from others has suggested that the performance of real SAA catalysts, which typically consist of SAA NPs dispersed on a high-surface-area oxide support, may be affected by additional factors, in particular the ease with which specific metals segregate to the surface and/or diffuse into the metal bulk upon exposure to various chemical environments. 30, 38-43.

The fact that one of the metals in alloys may segregate to the surface or diffuse into the bulk depending on the conditions and chemical environments is well known; a beautiful example was provided a few years ago by the Salmeron group, who showed using near-ambient-pressure X-ray photoelectron spectroscopy (NAP-XPS) that Rh-Pd core-shell NPs undergo reversible changes in composition and chemical state in response to oxidizing or reducing conditions: Rh segregates to the surface in a pure NO environment, whereas a more mixed-metal layer with significant amounts of Pd on the surface develops during NO + CO conversions.⁴⁴ In a case

involving hydrogenation catalysis, for the selective conversion of cinnamaldehyde, the Rh-Au bimetallic catalyst was shown to undergo segregation into Janus NPs during catalysis.⁴⁵ If the active metal in SAAs were to diffuse deep into the bulk, its activity may be hindered. For instance, the group of Crooks and coworkers proved that coating Pt NPs with a layer of Cu, to form Pt@Cu core-shell structures, leads to the inhibition of the electrochemical hydrogen evolution reaction (HER).⁴⁶ In a recent work of the Frenkel group and collaborators restructuring of Pd-Au nanoparticles with 8% of Pd was shown to result from the catalyst pretreatment (segregation and forming dimers and trimers of Pd atoms within the Au surfaces in O₂ atmosphere vs fragmentation of the ensembles into Pd monomers (SAAs) in H₂ atmosphere) and affect the H-D exchange activity.. It is therefore imperative to characterize the composition of the surface in bimetallic catalysts in situ to determine the true nature of the active sites. In this work we do that for the case of Cu-Pt bimetallic catalysts by combining the use of in situ infrared (IR) and X-ray (XAS) absorption spectroscopies during exposures to atmospheric pressures of different gases, both reactive (CO, H₂) and inert (He). Our results indicate that, indeed, selective metal segregation does occur as a function of temperature. The details are provided below.

2. Methods

A total of 10 CuPt_x/SBA-15 catalysts were prepared by using an incipient wetness impregnation method, using copper nitrate (Cu(NO₃)₂·3H₂O, Sigma-Aldrich, 98% purity) and chloroplatinic acid (H₂PtCl₄·6H₂O, Sigma-Aldrich, \geq 37.50% Pt basis), as reported previously.^{30, 31} In our nomenclature, x represent the molar fraction of Pt added to a constant 5 wt% Cu load, and was

varied from 0 (pure Cu) to ∞ (pure Pt). The physical characterization and pretreatment details of these catalysts have been provided before.^{30, 31}

The transmission Fourier-transform infrared (FTIR) spectra for carbon monoxide adsorbed on the CuPt_x/SBA-15 catalysts were performed using a homemade quartz IR cell capable of sustaining pressure of up to approximately 2 bar and of cooling or heating to temperatures within the range from 125 to approximately 700 K, and a Bruker Tensor 27 FTIR spectrometer equipped with a deuterated triglycine sulfate (DTGS) detector. 47, 48. About 15 mg of the catalyst was pressed into a self-supporting wafer, placed in the center of the transmission IR cell, and reduced in situ at 625 K under 500 Torr H₂ for 3 h. For the experiments carried out under vacuum, the cell was evacuated and cooled down to 125 K (using liquid nitrogen), after which the sample was exposed to 50 Torr of CO (Matheson Tri-Gas, ≥99.5% purity) for 0.5 h and the cell evacuated for 10 min. Spectra were recorded from 125 to 475 K, at 20 K intervals, as the sample and cell were warmed up, and corrected using background traces obtained under the same condition before adsorption. For the in situ CO IR titration experiments, the cell was cooled down to room temperature and evacuated, after which an initial IR spectrum was taken, to be used as the background reference. The CO gas was introduced to the appropriate pressure, and the indicated sequences of exposures and data acquisition followed. Reference spectra for the gas-phase CO were acquired by following the exact same procedure but without any catalyst in the IR cell. All spectra were acquired with a resolution of 2 cm⁻¹, and correspond to averages of 16 scans.

The *in situ* X-ray absorption spectroscopy (XAS) experiments were carried out at the Inner-Shell

Spectroscopy (ISS) beamline of the National Synchrotron Light Source II (NSLS-II) of Brookhaven National Laboratory. Approximately 25 mg of the catalyst was loaded onto a quartz tubing (O.D. = 2.4 mm, I.D. = 2 mm) and mounted in a Clausen cell.⁴⁹ Initial Cu and Pt *in situ* XAS spectra were acquired under a flowing atmosphere of pure He (20 mL/min) for reference, after which the gas feed was switched to pure H₂, to reduce the catalyst, and then to the gases indicated in the reported experiments, all at 1 atm: pure H₂ (20 mL/min), pure He (10 mL/min), or 25 vol% CO in He (20 mL/min total). In all cases, the Pt L₃-edge XAS data were collected in fluorescence mode and the Cu K-edge (taken but not reported here) XAS data were collected in transmission mode.

3. Results

Early indication that exposure of CuPt_x/SBA-15 catalysts to different gas environments may lead to metal segregation was provided by *ex situ* IR characterization experiments using carbon monoxide as a probe.³⁰ Figure 1 displays the IR spectra obtained in the C–O stretching region for all 10 catalysts after saturation with CO at 125 K. The data were acquired under vacuum, after pumping of the CO used for dosing, while the IR cell was slowly heated; the four panels provide results for four different temperatures (125, 225, 325, and 425 K). It is seen in Figure 1 that the main peaks for CO adsorbed on all of the CuPt_x/SBA-15 SAA catalysts (x = 0.001 to 0.75) at low temperatures are at frequencies in the 2100 - 2135 cm⁻¹ (main feature) and 2157 - 2170 cm⁻¹ (shoulder) ranges, blue-shifted as the Pt content in the catalysts is increased. These values are close to those seen with the pure Cu/SBA-15 catalyst, at ~2124 and ~2160 cm⁻¹

(Figure 1, left panel, top trace), and far from the much larger feature seen with the pure Pt/SBA-15 catalyst (bottom trace, peak at 2097 cm⁻¹). In fact, no signal that can be ascribed to CO adsorption on Pt atoms is seen in any of the alloy catalyst, with the possible exception of the broad feature seen around 2070 cm⁻¹ with the CuPt_{0.75}/SBA-15 sample. It is concluded that no Pt atoms are present on the surfaces of any of the CuPt_x/SBA-15 ($x \le 0.5$) within the detectability limit of the IR technique. In terms of the oxidation state of the Cu surface, we have, on the basis of the extensive studies available in the literature,⁵⁰⁻⁵⁵ assigned the main 2124 cm⁻¹ peak and the 2160 cm⁻¹ shoulder to adsorption on metallic and oxidized Cu, respectively;⁵⁵ it would appear that the catalysts is not yet fully reduced at the start of these experiments (it does become fully reduced upon heating in the presence of CO, see below).

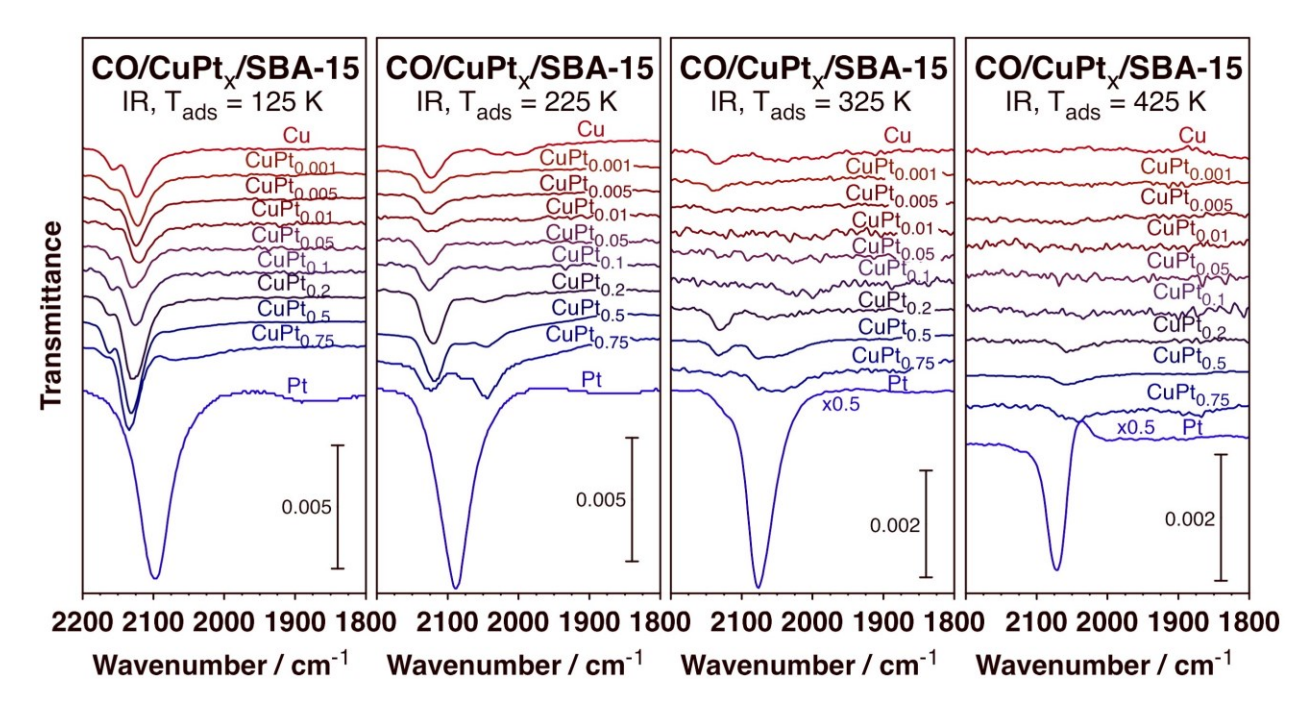


Figure 1. IR spectra for CO adsorbed on 10 different CuPt_x/SBA-15 catalysts (x = 0 to ∞) as a function of temperature: data for four values of T (125, 225, 325, and 425 K) are provided, each in a separate panel.

Heating to 225 K leads to some noticeable changes (Figure 1, 2nd-from-left panel). For one, the high frequency peak, associated with adsorption on oxidized Cu, is no longer evident in the spectra. It could be argued that CO bonding to those sites is weak and that, therefore, molecular desorption takes place at low temperatures, below 225 K. Alternatively, that adsorbed CO may react with the surface oxygen atoms and form CO₂, thus reducing the surface; the fact that the IR signal for gas-phase CO₂ increases upon heating of these samples (not shown) lead us to favor this second explanation. In any case, some CO desorption from metallic CO also occurs by 225 K, since the intensity of the main peak from all Cu/SBA-15 and CuPt_x/SBA-15 catalysts decrease. Particularly noteworthy is the evolution of a new peak in the low-frequency range for the samples with high (x \geq 0.2) Pt loads: that feature is weak and detected at 2050 cm⁻¹ in CuPt_{0.2}/SBA-15 but it grows and red-shifts with increasing Pt fraction in the bimetallic NPs, to 2045 cm⁻¹ in CuPt_{0.5}/SBA-15 and to 2044 cm⁻¹ in CuPt_{0.75}/SBA-15. This signal is most likely associated with CO bonded to Pt atoms, which must therefore segregate to the surface. Given that the observed frequencies are below the values reported for CO adsorption on either pure Pt surfaces (even at low coverages), 56-58 or supported Pt catalysts, 59 we conclude that the Pt atoms in our bimetallic catalysts may be atomically dispersed within the Cu matrix. frequencies have recently been reported for $CuPt_{0.39}/Al_2O_3^{60}$ and $AgPt_x/Al_2O_3^{61}$ SAA catalysts.

The third panel of Figure 1 shows the IR spectra recorded after heating to 325 K. By this temperature, most of the CO adsorbed on Cu is gone (notice the change of scale between the first two and the last two panels in Figure 1); the binding energy on pure Cu/SBA-15 is on the order of $\Delta H_{ads} = -82$ kJ/mol, and desorption in that case peaks at 245 K.⁵⁵ A small amount of CO on Cu is still detectable in some of the CuPt_x/SBA-15 samples, and the peak for CO adsorption on

Pt sites in the high-content bimetallic catalysts broadens and blue-shifts, possibly because the molecules no longer interact with other CO molecules bonded to adjacent Cu sites. Finally, by 425 K (Figure 1, right panel), only small peaks for CO bonded to Pt are seen, and only for the high-Pt-content cases (at 2058 cm⁻¹ with CuPt_{0.1}/SBA-15 and CuPt_{0.2}/SBA-15, and at 2042 cm⁻¹ with CuPt_{0.75}/SBA-15). It should be noted that the CO seen in these high-Pt-content catalysts, although persistent to higher temperatures than the CO adsorbed on Cu, still desorbs at temperatures below those seen on pure Pt/SBA-15; the Pt–CO binding is clearly stronger than that of Cu–CO, but not as strong as on non-alloyed Pt surfaces.

In the end, the data in Figure 1 evidence the ability of CO to draw the Pt atoms in CuPt_x/SBA-15 catalysts from the bulk to the surface as those are heated. Additional experiments were performed to test the reversibility of this behavior. Figure 2 shows the IR data collected with the CuPt_{0.5}/SBA-15 (top) and CuPt_{0.75}/SBA-15 (bottom) catalysts as they were saturated with CO and heated under vacuum three times in a row. The left panels show the results in the form of 3D "heat" plots: the x axis represents the frequency range and the y axis temperature, and the peak intensities are color-coded from low (blue) to high (red, with yellow for intermediate values); on the right side of Figure 2, representative IR traces are provided for low (125 K) and high (225 K) temperatures for the three cycles. The spectra for the first cycle mimic those seen in Figure 1, and demonstrate that, upon heating to 225 K or above, some CO adsorbed on Cu desorbs (all of the CO on the oxide sites plus approximately half of those on metallic Cu) and new Pt–CO sites develop, the consequence of Pt segregation to the surface. The data from the second cycle looks similar to that from the first: upon cooling down the catalysts and saturating them again with CO the peaks for CO bonded to CO reappear and the signals for adsorption on

Pt go away, but heating to 225 K again leads to the desorption of CO from Cu–CO sites and to the re-segregation of Pt to the surface. The results recorded during the third cycle are somewhat different, pointing to a possible irreversible change in the Cu-Pt bimetallic NPs, but the general trends are still the same, namely, the dominance of CO adsorption on Cu is restored at low temperatures but gives way to CO bonding to segregated Pt after heating the samples up. Also to notice here is the observation that the Pt–CO still desorbs by 300 K, a temperature clearly higher than that for Cu–CO but much lower than when CO desorbs from pure Pt surfaces (≥ 350 K).⁶²⁻⁶⁴

CO/CuPt_x/SBA-15 IR Absorption Spectra Surface Composition vs. Exposure Cycling

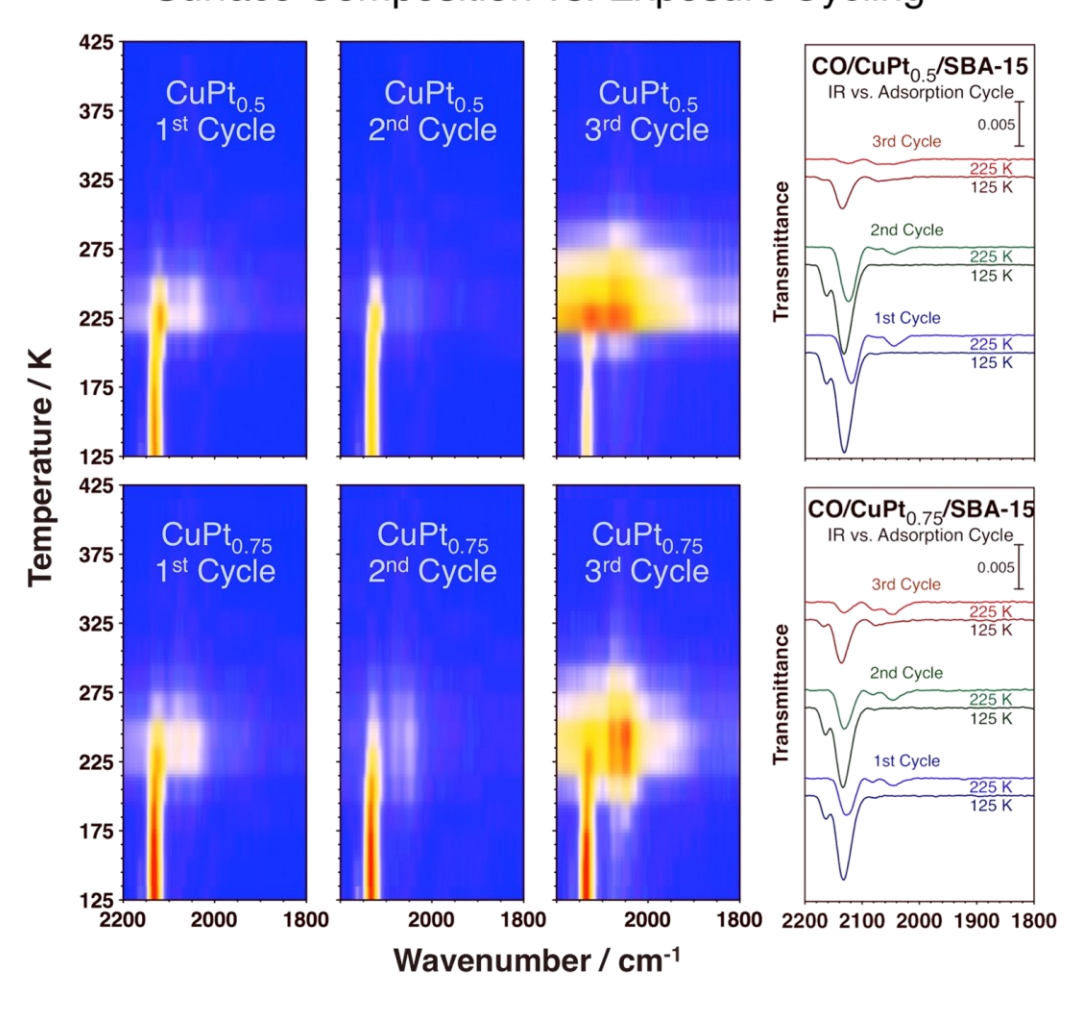


Figure 2. IR spectra for CO adsorbed on CuPt_{0.5}/SBA-15 (top) and CuPt_{0.75}/SBA15 (bottom)

catalysts, recorded as a function of heating temperature during 3-cycle dose-pump-heat sequences. The left panels correspond to 3D "heat" plots, whereas the right figures report representative spectra for low (125 K) and high (225 K) temperatures during each of the three cycles.

The data presented so far were acquired ex situ, that is, under vacuum after having pumped the CO atmosphere from the IR cell. More relevant to the main goal of this project was the investigation of the behavior of the Cu-Pt bimetallic NPs in situ, in the presence of a gas phase. To achieve that, IR spectra were recorded under similar conditions, at different temperatures and in the presence of a fixed pressure of CO, both in the presence and in the absence of the catalysts in the path of the IR beam. This way, the contribution from the gas phase species detected in the latter could be subtracted directly from the former to extract the peaks attributable to the adsorbed species. This approach is feasible because when dealing with supported catalysts the area of the reactive surfaces is high and the total number of adsorbed molecules probed can reach values close to those of the gas-phase species. Figure 3 displays an example of the results acquired this way, in this case for the in situ titration of Cu and Pt sites in a CuPt_{0.2}/SBA-15 catalyst as a function of temperature using 10 Torr CO. Several features are seen, in particular a peak at 2137 cm⁻¹ at low temperatures (295 K) corresponding to adsorption on copper surfaces. Interestingly, that feature slowly disappears with increasing temperature, presumably because CO binds weakly to Cu and desorbs at low temperatures, and is replaced by a new signal around 2050 cm⁻¹ easily associated with Pt sites. A smaller and broader feature is already seen in this frequency region at low temperature, but the peak sharpens and grows at 495 K. It appears that the Pt atoms in the CuPt_{0.2}/SBA-15 catalyst, which may initially be located in the subsurface region, reversibly segregate to the surface at higher temperatures driven by the CO atmosphere.

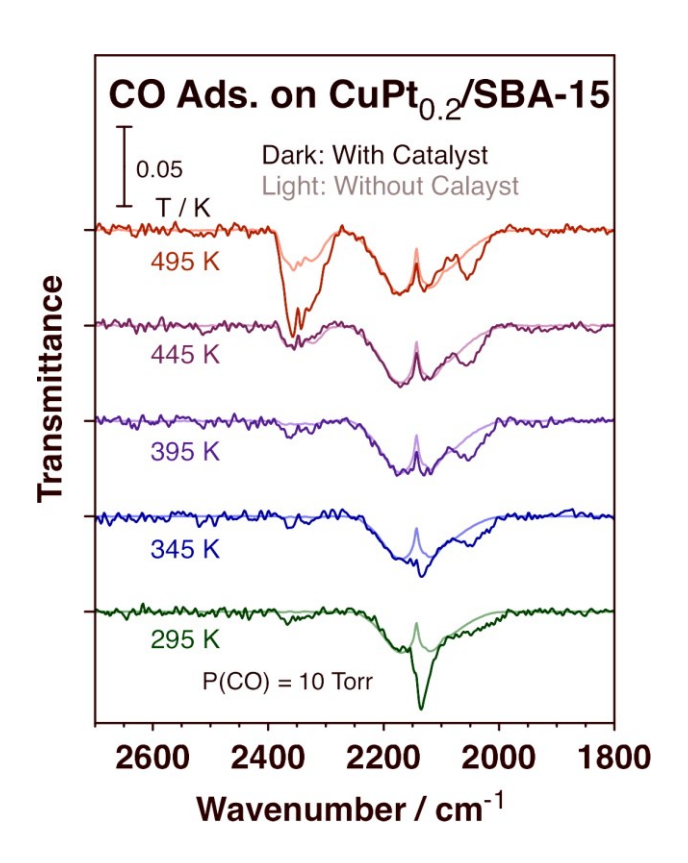


Figure 3. In situ IR spectra of CO adsorbed on a CuPt_{0.2}/SBA-15 catalyst as a function of temperature. The spectra were taken in the presence of 10 Torr of CO in the gas phase in order to maintain a steady-state coverage of adsorbed CO at temperatures typical of catalytic processes. Additional reference spectra were acquired without the catalyst (light traces) in order to subtract the contribution from the gas phase to the spectra.

Similar experiments were carried out with other $CuPt_x/SBA-15$ catalysts in order to characterize the behavior of these catalysts as a function of Pt content. Key results are displayed in Figure 4: spectra recorded under 50 Torr CO at room temperature (left panel), after heating to 495 K (center), and after cooling back down to room temperature again (to test the reversibility of the temperature-induced changes; right) with 8 catalysts, namely, the pure Cu/SBA-15 and Pt/SBA-15 samples, and $CuPt_x/SBA-15$ with x = 0.001, 0.005, 0.01, 0.05, 0.1 and 0.2. Here, the spectra after subtraction of the gas-phase contribution are shown for clarity. Similar features to those reported in Figure 3 were seen, namely, the peaks in the 2120 - 2130 and 2040 - 2080 cm⁻¹

associated with bonding to Cu and Pt atop sites, respectively, and also an additional small feature at 2200 cm⁻¹ most likely due to adsorption on oxidized Cu sites. A few trends become clear upon observation of this figure. For one, most (although not all) of the CO bonded to Cu desorbs by 495 K, due to the weak binding energy of those surface species. Not all of the CO is gone, however: the peak for Cu–CO retains approximately 20 - 30% of its initial intensity in going from 295 to 495 K, a reflection of the equilibrium that is established between the adsorbed and gas-phase molecules. In fact, the steady-state CO surface coverage can be increased by increasing the gas-phase CO pressure, as we have already demonstrated for the case of Cu/SBA-15 in a previous publication, ⁵⁵ and as it can be seen in Figure 5, to be discussed later.

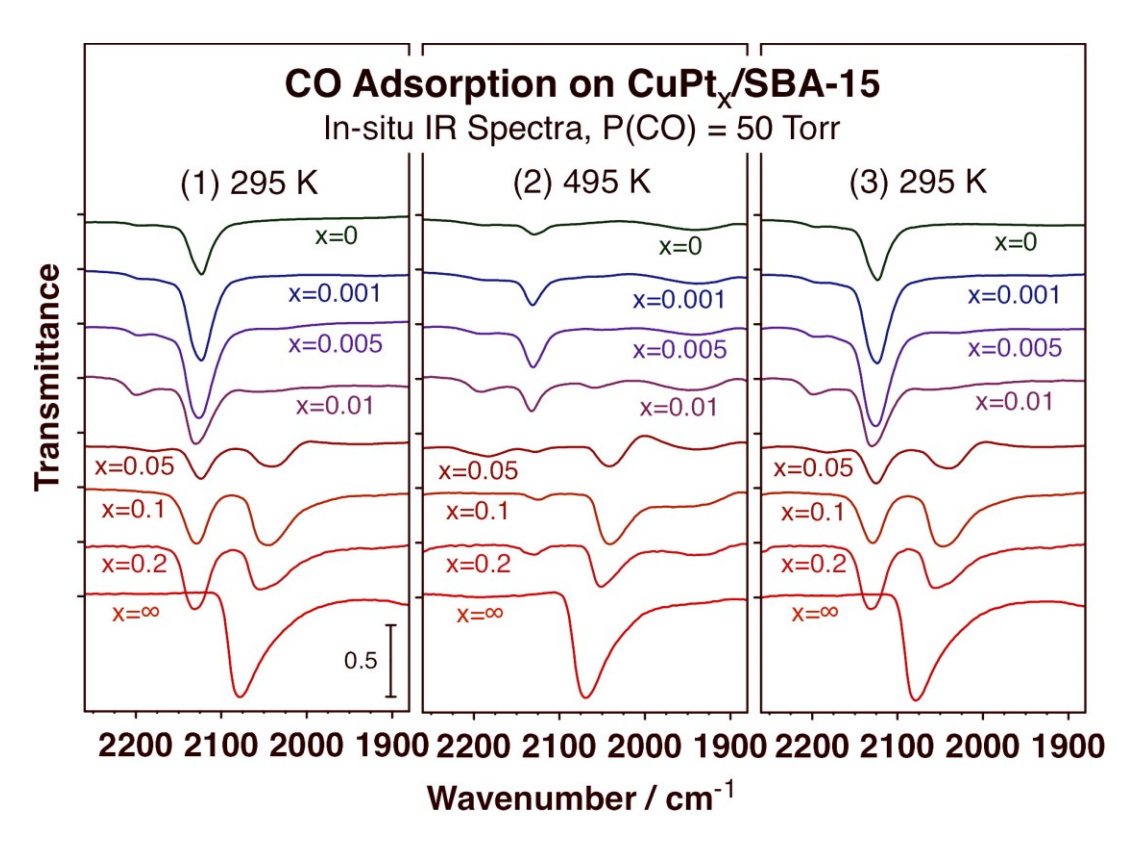


Figure 4. In situ IR spectra of CO adsorbed on a family of CuPt_x/SBA-15 catalyst as a function of Pt content (x), in the presence of 50 Torr of CO in the gas phase (after subtraction of the gas-phase contribution). Three panels are provided, showing the traces recorded at 295 K (left), after heating to 495 K (center), and upon cooling back down to 295 K again (right). These temperature cycling was designed

to test the reversibility of the changes seen as a function of temperature.

The behavior of the IR peak associated with the Pt–CO species is somewhat different. With the more diluted alloys, for $x \le 0.01$, the Pt content is low, and therefore the peak due to adsorption on Pt atoms is weak, as expected. What is significant is the fact that it is only seen at high temperatures, in the traces recorded at 495 K; the peaks at 2060 cm⁻¹ (with CuPt_{0.01}/SBA-15) and 2035 cm⁻¹ (CuPt_{0.005}/SBA-15) appear only while heating the reactor, and go away again once the sample is cooled back down to room temperature. In addition, the value of the frequencies are low but do not follow the same trends seen with higher Pt content; notice in particular that the C–O stretching of the Pt–CO species in CuPt_{0.01}/SBA-15 (2060 cm⁻¹) is higher than with CuPt_{0.05}/SBA-15 (2040 cm⁻¹), in spite of the fact that the intensity of the peak in the former case is much lower than in the latter. The Pt surface atoms in the diluted bimetallic catalysts appear to behave differently than in the catalysts with higher Pt content, and are likely to be isolated, as expected in SAAs. The most relevant observation here is the fact that, as already suggested by the *ex situ* IR experiments, adsorbed CO appears to help draw the Pt atoms toward the surface at high temperatures, and reversibly drive them into the bulk at low temperatures.

For the alloys with high Pt content, $x \ge 0.05$, the peak position associated with CO bonded to Pt blue-shifts significantly with increasing Pt content in the Cu-Pt bimetallic NPs, from 2040 cm⁻¹ in CuPt_{0.05}/SBA-15 to 2070 cm⁻¹ in Pt/SBA-15. These shifts are accompanied by related increases in peak intensity, due to increases in the surface coverage of Pt atoms, and can be explained by an increase in dipole-dipole intermolecular interactions, as has been reported and amply discussed in studies with Pt single crystals.⁶⁵⁻⁶⁷ It seems that at these high Pt loadings CO

behaves as in regular alloys with multi-atom Pt assemblies on the surface; these are not SAA catalysts. It is interesting to point out that the peak shifts seen in the IR feature for Cu–CO sites are well less marked, suggesting that the surfaces of these catalysts are still dominated by Cu. It is also worth noticing that in Figure 4 both the peak positions and the peak intensities of the feature for Pt–CO do not change significantly upon heating or cooling of the catalysts. Some sharpening and growth of that peak was seen in some cases, more clearly in the data in Figure 3 (the data in Figures 3 and 4 are from different experiments, performed at different CO pressures), but the changes are not as significant as with the more diluted alloys.

That lack of sensitivity of the IR features to changes in temperature with the high-Pt content catalysts as explore in more detail next. It was found that thermal treatment of the high-Pt-content catalysts in the presence of a gaseous atmosphere still leads to intermetallic atom mobility within the individual NPs, only that the behavior is complex as it depends on both temperature and CO pressure. This can be seen more clearly in Figure 5, where CO IR spectra are shown for CuPt_{0.2}/SBA-15 as a function of temperature for several CO pressures. Peaks for both Cu–CO and Pt–CO sites are seen in all cases, but their absolute and relative intensities as well as their shapes change with varying conditions. The signals from the Cu–CO species go up in intensity with CO pressure, and down with increasing temperature, both expected behavior. In the case of the Pt sites, however, the trends are reversed. Interestingly, in general, the peak for Pt–CO is more intense and sharper at the lower CO pressures, with the one exception of the 1 Torr CO at 495 K (in that case, the CO may have been consumed in oxidation reactions). These results suggest that at low temperatures higher gas pressures induce partial segregation of Pt into the bulk of the bimetallic NPs. It is also seen that more surface Pt is detected in going from 295

K to 395 K, following the same trend discussed above for the more diluted alloys, but then less Pt–CO is seen at 495 K. It could be thought that Pt may diffuse back into the bulk in this latter case, but in fact we believe that the observed behavior is the result of a thermodynamic effect, as the rate of CO desorption increases with T and leads to lower steady-state surface CO coverages. In the end, the *in situ* IR data are all consistent with Pt diffusing into the bulk in the presence of CO at low temperatures and segregating back to the surface as the catalysts are heated.

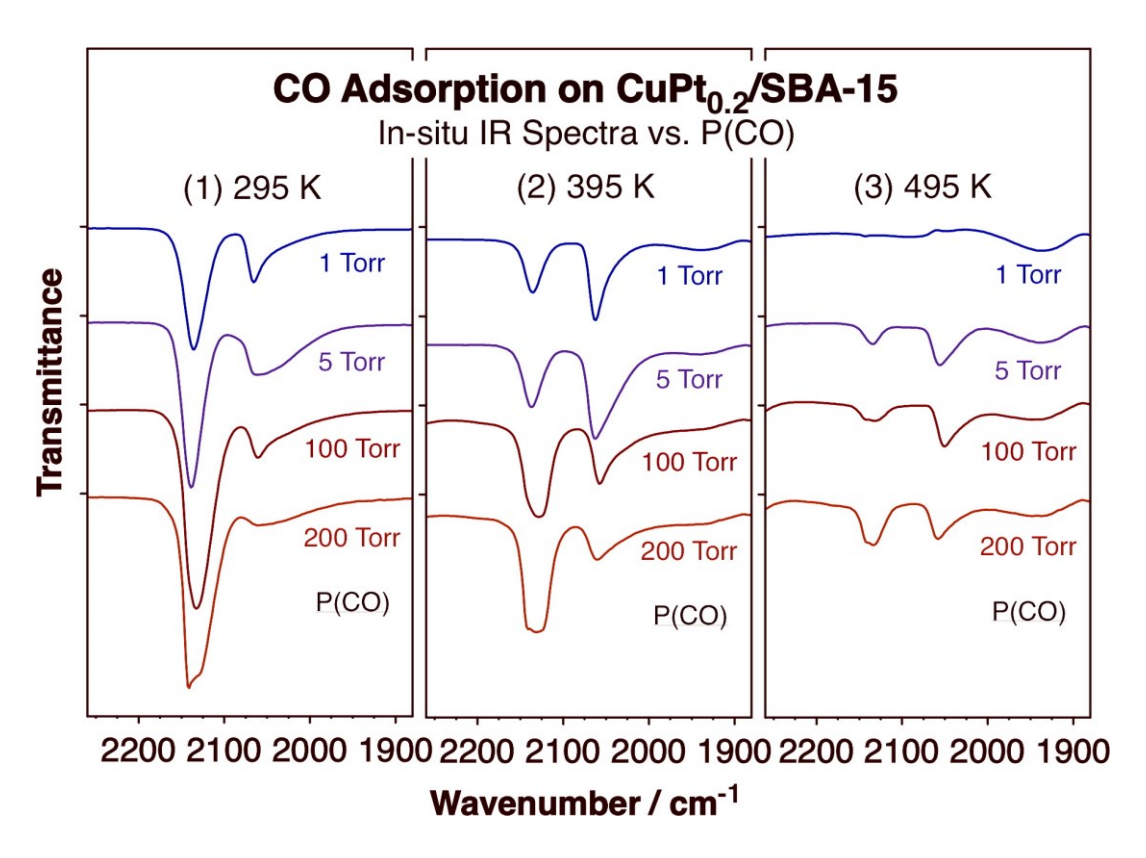


Figure 5. *In situ* IR spectra of CO adsorbed on the CuPt_{0.2}/SBA-15 catalyst as a function of CO pressure (after subtraction of the gas-phase contribution). Three panels are provided, showing the traces recorded at 295 K (left), 395 K (center), and 495 K (right).

The IR characterization of our Cu-Pt bimetallic catalysts has been carried out by using CO as a probe molecule, in a CO environment. CO is an important reactant in many catalytic processes,

but is to be avoided in hydrogenation reactions. More relevant in those cases is the behavior of the surface of the catalyst under reducing conditions, H₂ atmospheres if possible. Unfortunately, adsorbed hydrogen is virtually invisible in IR, at least in supported catalysts (vibrational spectra, taken using high-resolution electron loss spectroscopy –HREELS-^{68, 69} or inelastic neutron scattering –INS-,⁷⁰⁻⁷² have been reported with some Pt systems). Instead, an attempt was made here to test the performance of the CuPt_x/SBA-15 catalysts under hydrogen atmospheres in an indirect way. Two types of experiments were carried out (Figure 6). In the first, the catalyst (CuPt_{0.1}/SBA-15 in this case) was first reduced in a H₂ atmosphere (200 Torr at 495 K) and then probed by adding a small amount of CO to the gas at room temperature (300 K; Figure 6, left panel): after an initial addition of 0.2 Torr CO no adsorption could be detected, but upon adding another 0.2 Torr CO, two peaks were clearly seen at 2127 and 2029 cm⁻¹ corresponding to the C-O stretching mode of CO adsorbed on atop sites of metallic Cu and Pt surfaces, respectively. The interesting observation here is that the intensities of both features increase after each of two consecutive cycles of heating the sample from 300 K to 495 K and cooling it back to 300 K. The growth of the peak for Cu-CO is explained by the reduction of the Cu₂O surface layer that presumably was not fully removed during the H₂ treatment by the added CO, and to the resulting creation of additional metallic Cu sites available for CO uptake; further confirmation of this interpretation is given by the growth of the peaks in the 2300 - 2400 cm⁻¹ range due to gas-phase CO₂, the product of CO oxidation. Importantly, the signal for the Pt-CO site grows faster relative to that for Cu-CO, suggesting that H₂ may help draw the Pt atoms to the surface as a result of the high-temperature cycling.

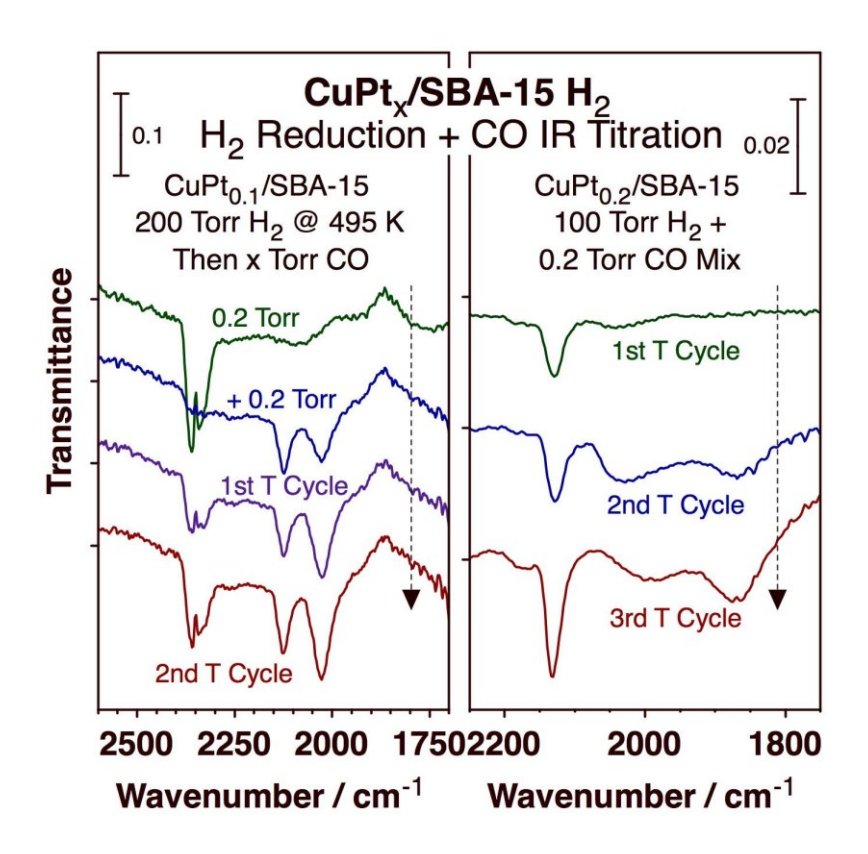


Figure 6. IR spectra of CO adsorbed on $CuPt_x/SBA-15$ catalysts after different H_2 reduction treatments. Left: Spectra for $CuPt_{0.1}/SBA-15$ reduced in a 200 Torr H_2 atmosphere, after adding a small amount (0.2 Torr twice) of CO and cycling the temperature to 495 K and back to 300 K. Right: Data for $CuPt_{0.2}/SBA-15$ exposed to a 100 Torr $H_2 + 0.2$ Torr CO mixture; the spectra were obtained after each of three consecutive heating cycles to 495 K and cooling back down to 300 K.

The second set of experiments were done using H₂ + CO gas mixtures, 100 Torr H₂ + 0.2 Torr CO in the example shown in the right panel of Figure 6 (which corresponds to a CuPt_{0.2}/SBA-15 catalyst). The peak at 2132 cm⁻¹ for CO adsorption on metallic Cu is again seen to grow upon cycling to 495 K and back, a procedure that was carried out three times in this example. The same explanation applies to this system, namely, that the small amount of CO added to the H₂ gas helps complete the reduction of the metal NPs, removing the residual Cu₂O layer present on the surface under H₂ atmospheres at low temperatures. Unfortunately, in this case adsorption on Pt atoms was not evident at any stage of the experiments. In the end, small amounts of CO were

used in both examples in order to minimize its interference in the behavior of the catalyst under H₂ atmospheres, but a CO reducing effect was nevertheless identified. Some interference is unavoidable, more obviously perhaps in the second example, where the chances of surface site poisoning are greater. An alternative experimental approach is needed to probe the surfaces of these catalysts *in situ* in atmospheres not containing CO. We addressed this challenge by incorporating XAS to our studies.

XAS characterization of our catalysts can provide information on several aspects of their physical properties. In Figure 7, we report data recorded *in situ* under different gas atmospheres in the near-edge region (XANES) around the Pt L₃-edge in order to probe the electronic properties of the Pt atoms. The two low traces in the left panel of that figure contrast the spectra obtained for a Cu_{0.8}Pt_{0.2}/SBA-15 catalyst as is, before any pretreatment, versus that for a reference PtO₂ sample. The similarity between the two indicates that, initially, the platinum in our alloy catalyst is in an oxidized state, most likely in a Pt⁴⁺ state. The match of the two spectra is not complete because of the dispersed nature of the Pt atoms within the Cu-based matrix in the supported NPs of the catalyst.

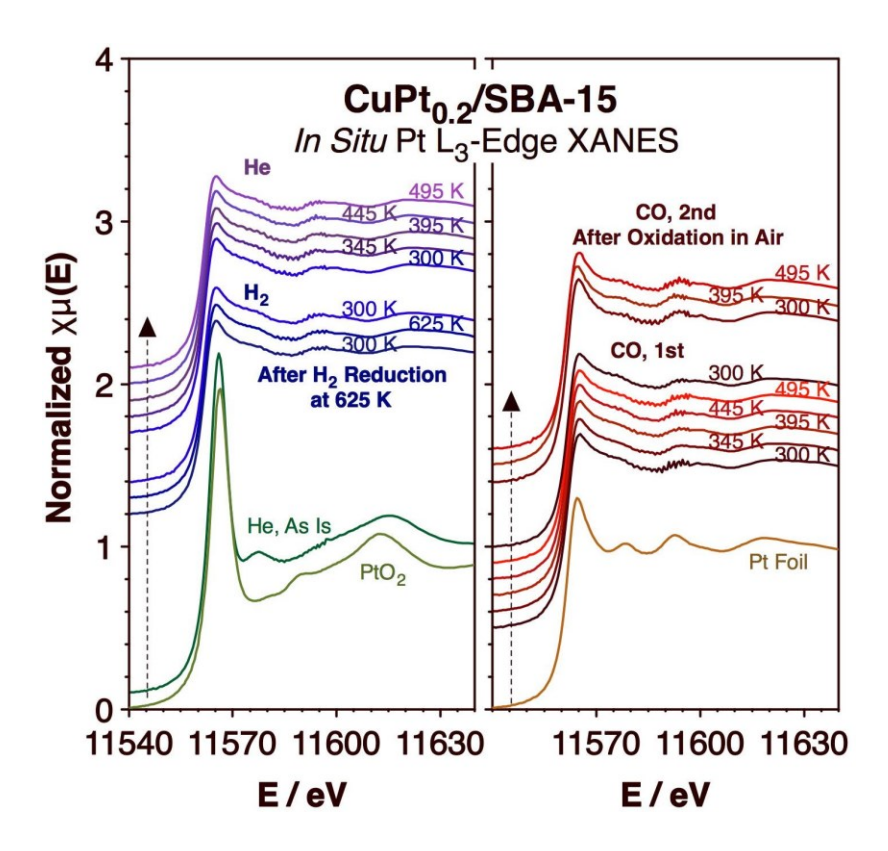


Figure 7. In situ X-ray absorption near edge spectra (XANES) recorded around the Pt L₃ edge for a CuPt_{0.2}/SBA-15 catalyst exposed to different gases (H₂, He, CO) and cycled between 300 and 495 K. Reference spectra from PtO₂ (left) and a Pt foil (right) are also provided at the bottom for reference. No detectable changes in Pt electronic properties were seen in any case after initial reduction of the catalyst.

The reminder of the traces reported in Figure 7 corresponds to the Pt L₃-edge XANES of the same CuPt_{0.2}/SBA-15 catalyst obtained after high-temperature (625 K) pretreatment in H₂. The data are grouped to highlight the behavior of the catalyst as they were subjected to heating-cooling cycles (from 300 K to 625 K and back) under different gas atmospheres: H₂ (left panel, 3rd to 5th traces, counting from the bottom), He (left panel, 5 top traces), and CO (right panel, 2nd to 6th traces from the bottom). Interestingly, all these spectra look the same, indicating that the electronic properties of the Pt atoms in the bimetallic catalyst are not significantly affected by the nature of the gas or the temperature (within the range tested here). Comparison with a spectrum obtained with a reference Pt foil (right panel, bottom) points to the fact that the Pt

atoms are most likely in a zero-valent state; the peaks are seen at approximately the same energies, and their lower intensities can again be explained by the dilute nature of the Pt within the Cu-based alloy. Even after exposure to air (at room temperature, 30 min; right panel, top three traces), not much change is detected: a minor oxidation may be detectable then, but the Pt atoms in that case are readily re-reduced to metallic Pt upon re-exposure to CO.

Additional information on the local environment surrounding the Pt atoms in our catalysts can be extracted from analysis of the extended X-ray absorption fine structure (EXAFS) in the spectra at the Pt L₃-edge region. In Figure 8, the EXAFS radial distribution functions (the Fourier transform magnitudes of the k^2 -wei]ghted EXAFS spectra) are reported for the CuPt_{0.2}/SBA-15 catalyst while cycling the temperature from 300 to 495 K and back under CO (left panel) and He (right) atmospheres. In all cases, the main peak (uncorrected for the photoelectron phase shift) is seen at R \sim 2.23Å, which corresponds to individual Pt atoms bonding to Cu neighbors; it suggests that the Pt is (partially) alloyed with Cu. A shoulder is also seen around 2.9 Å, pointing to the fact that some Pt atoms are directly bonded to other Pt atoms. The peak intensities decrease with increasing temperature, but that can be mostly accounted for by the so-called Debye-Waller factor that reflects the attenuation of X-ray scattering caused by thermal motion. Noticeably, similar behavior is seen in CO versus He atmospheres.

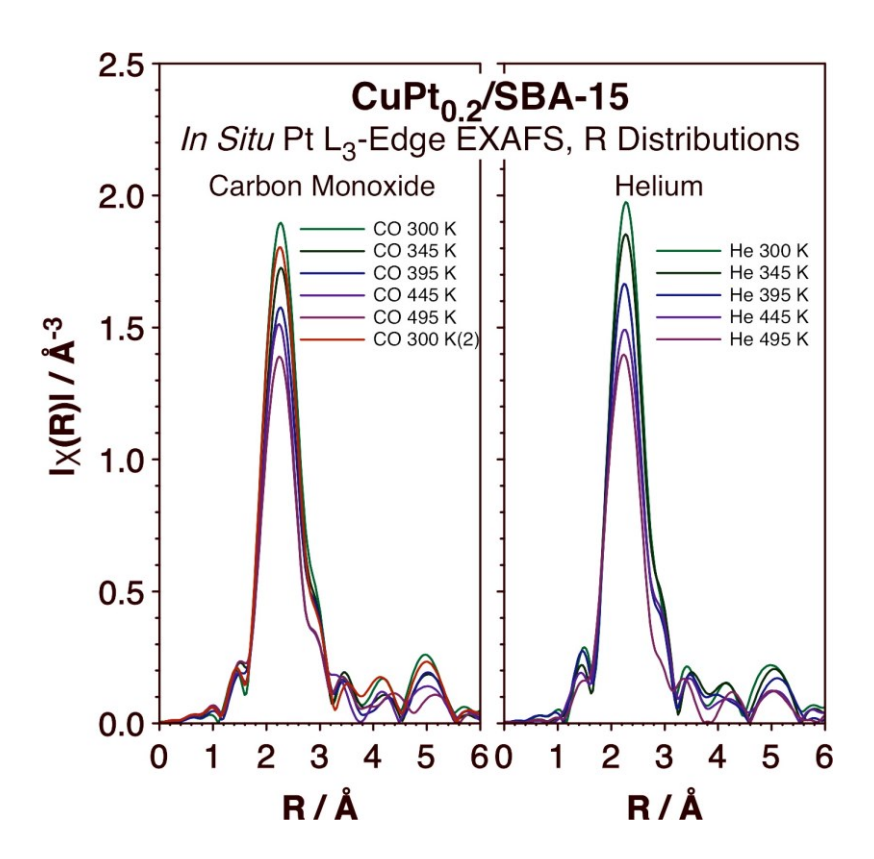


Figure 8. Pt L₃-edge EXAFS radial distributions obtained for our CuPt_{0.2}/SBA-15 catalyst *in situ* in CO (left) and He (right) atmospheres as a function of temperature, which was cycled between 300 and 495 K.

Figure 9 shows the results from processing of the EXAFS data to extract quantitative parameters on the coordination sphere around the Pt and Cu atoms, specifically on coordination numbers (left, CN) and bond distances (right, d) as a function of temperature under both CO and He atmospheres. Data are reported for data from both the Pt L₃ and Cu K edges (the raw data for the Cu K edge are not shown). The coordination number around the Cu atoms hovers around 10-11 in all cases, almost all to other Cu atoms (red lines and symbols). This number is just shy of the value of 12 expected in bulk Cu, a reflection of the small size of the NPs and to the resulting existence of a detectable fraction of Cu atoms in lower-coordination surface sites. Using a back-of-the-envelope calculation, since in 5 nm spherical NPs (the average size in our CuPt_{0.2}/SBA-15

sample)³¹ the fraction of atoms on the surface is approximately 25%, an average CN of 6 for those (it is 9 in the (111) plane) results in an average total CN of 10.5, within the range measured here. There is a slight decrease in CN at 495 K, which we associate with the higher coordination of Cu atoms to Pt atoms highlighted by the changes in CNs for Pt discussed next. The Cu–Cu bond distances are also within the value measured for bulk Cu. (2.542 Å).

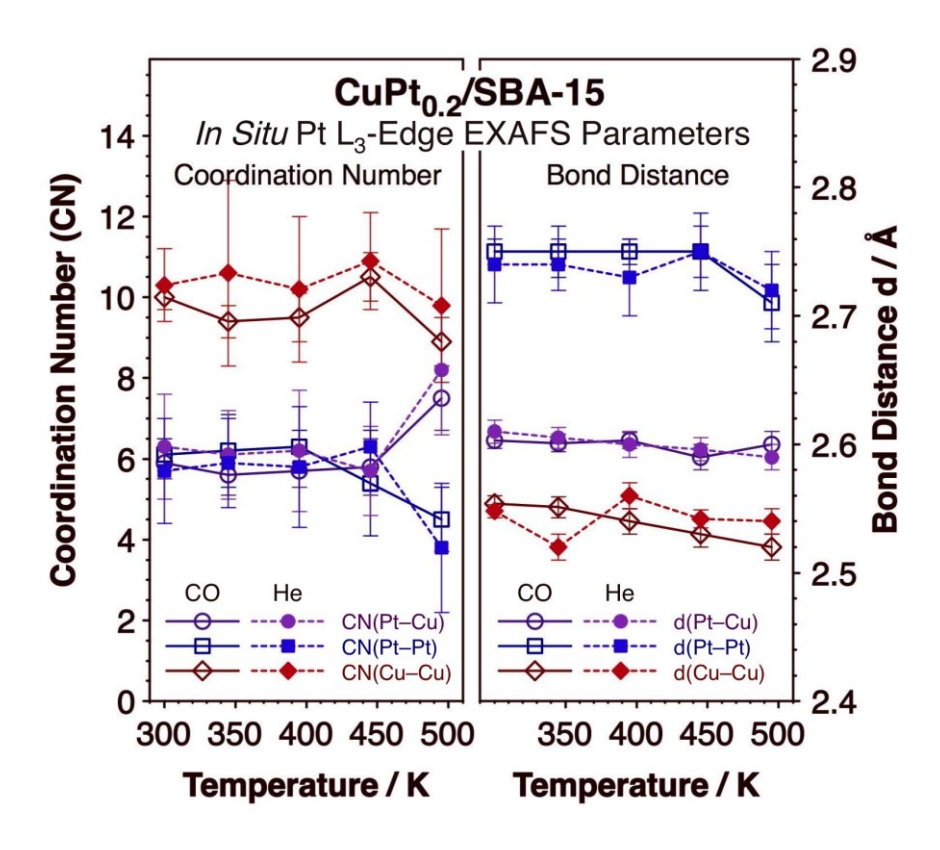


Figure 9. Coordination numbers (CN, left panel) and bond distances (d, right) extracted from analysis of the EXAFS data obtained at the Pt L₃ and Cu K edges (the latter not shown) for the CuPt_{0.2}/SBA-15 catalyst under either CO or He environments, all as a function of temperature.

More relevant to our discussion is the environment surrounding the Pt atoms. Again, the behavior seen for those atoms as a function of temperature are similar in the CO and He atmospheres. In both cases, the coordination around individual Pt atoms is split about evenly, ~

6:6, between Cu and Pt neighbors for temperatures up to 445 K. At 495 K, however, the Pt atoms are surrounded by a significantly larger number of Cu neighbors, at the expense of Pt–Pt pairs (Cu:Pt ~ 8:4). At the very least, this indicates some mobility of the Pt atoms within the bimetallic NPs induced by heating in a gaseous atmosphere. The changes also point to better Cu-Pt mixing at high temperatures, consistent with the CO IR data, and can be explained by segregation of Pt to the surface. The total CN around the Pt atoms adds up to approximately 12 in all cases, as expected for atoms in the bulk, but the lower values expected from having a fraction of the Pt atoms on the surface are within the experimental errors of the EXAFS data. There are still some Pt–Pt bonds in all cases, with bond distances slightly lower than that seen in the Pt foil reference (2.764 Å), and there also seem to be a slight contraction of that bond at 495 K. Incidentally, all of these changes proved to be reversible, as the structural parameters return to the initial values upon cooling of the catalyst back to room temperature.

4. Discussion

The main purpose of this research has been to characterize the behavior of CuPt_x/SBA-15 bimetallic catalysts *in situ* in the presence of atmospheric pressures of reactive and non-reactive gases. Because of their potential use in selective catalysis, in particular to promote selective hydrogenation conversions, the surface chemistry of the Cu-Pt bimetallic combination has been characterized extensively under controlled vacuum conditions (as mentioned in the Introduction). However, much less is known about its performance under realistic catalytic conditions. It is well known that both temperature and chemical environments can induce segregation of one or

more components of metal alloys toward the surface, and if so, change the nature of the catalytic surface. In the case of single-atom alloy (SAA) catalysts in particular, the placement of the minority component, on the surface versus dissolved inside the bulk, is expected to determine the mechanism by which reactions occur on such catalysts. Here we have investigated the specific case of Cu-Pt bimetallics, but these issues are general. *In situ* characterization of SAA catalysts is required to develop a picture of the nature of the surface that promote the catalytic reactions.

One of the clear conclusions of this work is that, indeed, the presence of a gaseous atmosphere leads to the thermally promoted diffusion of Pt within the Cu-Pt bimetallic NPs. In fact, even under vacuum a reactive gas such as CO can cause the segregation and/or desegregation of Pt atoms in those catalysts. Specifically, Figure 1 shows that, at least for high-content CuPt_x/SBA-15 catalysts ($x \ge 0.2$), binding of CO to Pt atoms cannot be detected at 125 K but it is seen to develop at temperatures as low as 225 K. This change indicates that the Pt atoms diffuse to the surface in between those two temperatures, likely aided by the presence of CO molecules on the surface. The binding of CO on the new sites is weaker than on pure Pt, but it is clearly stronger than on Cu/SBA-15. Another important observation regarding the changes of the CuPt_x/SBA-15 catalyst upon thermal cycling after exposure to CO is that the Pt segregation seen in Figure 1 is reversible; cooling the catalysts back down to room temperature followed by CO re-dosing leads to the disappearance of the IR features associated with CO adsorption on Pt (Figure 2). By and large, this behavior is reproduced during multiple CO-dosing/heating cycles.

A similar behavior was observed *in situ* in the presence of CO atmospheres, as indicated by the IR data in Figures 3, 4, and 5: clear peaks are seen at 2137 and 2050 cm⁻¹ at 295 and 495 K with

CuPt_{0.2}/SBA-15 clearly originating from surface species and easily assignable to CO bonding to Cu and Pt sites, respectively. Additionally, the changes seen upon heating and cooling of the CuPt_x/SBA-15 catalysts are, again, reversible. It should be indicated that in the catalysts containing high Pt loadings ($x \ge 0.05$) CO adsorption on Pt was seen at all temperatures; it is only with the diluted SAA catalysts ($x \le 0.01$) that no surface Pt is detected at low temperatures and reversible segregation of Pt to the surface is clearly observed at high temperatures, possibly driven by bonding to CO. This does not indicate that segregation does not occur with the high-Pt-content catalysts, only that in those cases the behavior is masked by the combined response of the bimetallic NPs to changes in both temperature and CO pressure.

Complementary information could be extracted from *in situ* XAS experiments. The XANES data reported in Figure 7 for CuPt_{0.2}/SBA-15 does not show much change in the electronic structure of Pt as a function of temperature or the nature of the gas surrounding the surface of the catalyst, consistent with the IR experiments. The main conclusion that can be driven there is that the features in the XANES traces with the bimetallic catalysts are much less defined than in pure Pt samples, suggesting good mixing with the Cu matrix and broadening of the Pt d band. On the other hand, analysis of the EXAFS data in Figures 8 and 9 does highlight a critical structural transition in CuPt_{0.2}/SBA-15 upon heating to 495 K. Specifically, the coordination sphere around the Pt atoms exhibit approximately the same number of Pt and Cu neighbors at low temperatures, but a significant increase in Cu–Pt bonds, at the expense of Pt–Pt pairs, is seen after heating to 495 K. This transition was observed in both reactive (CO) and un-reactive (He) atmosphere, and was found to be reversible, with the atoms redistributing back to their original configuration upon cooling back down to room temperature.

The high coordination number of Pt bonding to other Pt atoms at low temperature indicates that Pt must form large ensembles within the bimetallic NPs. Two possible models can be conceived to explain the results: either Pt forms small clusters within the larger Cu-Pt NPs, or, more likely, it may form shells, in a layered distribution of the metals within the NPs. The detection of CO adsorption in the IR experiments indicates that some Pt atoms are present on the surface of the catalyst at all temperatures, but the majority of the Pt may still be located in the sub-surface at low temperatures, perhaps separated by an intermediate Cu layer. After heating to 495 K, on the other hand, the CN for Pt-Pt pairs is significantly reduced, pointing to a better intermixing of the two metals. In addition, the CO IR peak associated with bonding to Pt becomes somewhat larger and sharper (Figure 3), possibly because of a higher coverage of Pt on the surface but in a better dispersed fashion. Old reports on the structure of Cu-Pt bimetallic samples provide support for this interpretation of the data, in that: (1) Cu and Pt are completely miscible in both bulk and NP forms, 73 and (2) the superlattice of Cu-Pt alloys is characterized by successive alternating Cuonly and Pt-only layers.⁷⁴ More relevant to the understanding of our results, Cu-Pt alloys are known to transition from solid solutions at high temperatures to a number of ordered structures at low temperatures. 75, 76 For an x = 0.2 composition (Pt molar fraction) this transition has been reported to take place at $T \ge 900$ K, but that is in bulk samples; the thermodynamics of NPs is expected to be different. In fact, several layered structures with surface Pt rows and/or subsurface Pt sheets have been shown to be stable in CuPt_x NPs by density-functional theory (DFT) calculations.^{77, 78} In addition, we suggest that the interaction of the bimetallic NPs with gases may help lower the temperature of the transition. Importantly, the transitions reported here were seen with both CO and He atmospheres, which means that the strong binding of CO to Pt may not be the dominating force driving them.

Changes in surface chemistry due to the preferential segregation of one element in bimetallic NPs has been recognized in the past, as discussed in the Introduction, and some specific examples have already been reported for Cu-Pt and similar cases. For instance, high-temperature CO-induced segregation of Pt atoms in Pt-doped Cu(111) surfaces has been identified by NAP-XPS.³⁹ The same behavior was seen with Pd/Ag(111),⁴² but not with Pt/Cu(111) when H₂ is used instead of CO.⁴³ It is also interesting to note that no isotope scrambling within H₂-D₂ mixtures was detected in experiments with CuPd_x alloy films at any temperature below ~ 550 K until a ~ 15 mol % Pd content was reached, a result that implies than no Pd atoms are accessible on the surface of diluted alloys for this catalysis.²³ Even under UHV, CO oxidation on Pt-doped O-dosed Cu(111) surfaces has been shown to lead to the diffusion of the Pt atoms underneath the Cu–O layer,⁷⁹ a behavior consistent with our temperature-dependent IR observations reported in Figures 1 and 2.

5. Conclusions

A synergy between Cu and Pt in Cu-Pt bimetallic catalysts was evidenced by their behavior both upon the uptake of CO under vacuum and their exposure to atmospheric pressures of either CO or He. CO adsorption on CuPt_x/SBA-15 catalysts only involves bonding to Cu sites at low (125 K) temperatures regardless of the Pt content (the x value), indicating the absence of Pt atoms on the surface (Figure 1, left). Pt segregation becomes evident after heating to 225 K for $x \ge 0.2$ by

the growth of a new peak in the IR spectra around 2044 - 2050 cm⁻¹ (Figure 1, second-from-left) but CO adsorption on those sites is still weaker than in pure Pt, desorbing at lower temperatures (Figure 1, two right panels). The low frequency of the peaks for the Pt–CO IR sites suggest atomic dispersion, as expected in single-atom alloy (SAA) catalysts, and the Pt segregation is partially reversible under the vacuum conditions of these experiments, as CO readsorption at room temperature leads to the disappearance of the IR feature for Pt–CO IR seen at the higher temperatures (Figure 2).

Pt surface segregation at high (495 K) temperatures is also observed under a CO atmosphere, evidenced by the growth of a new peak around 2050 cm⁻¹ in the *in situ* IR data (Figure 3). The absence of CO adsorption at low temperatures and the reversibility of the Pt segregation to the surface at high temperatures are easy to see in diluted SAA CuPt_x/SBA-15 catalysts ($x \le 0.01$; Figure 4). With bimetallic catalysts with higher Pt content some Pt–CO sites can be detected even at low temperatures (Figure 4), but some Pt diffusion in and out of the surface still occurs, only that it is highly dependent on the temperature and CO pressure used (Figure 5). The possible Pt atom mobility within Cu-Pt NPs in the presence of H₂ atmospheres was also probed indirectly with *in situ* IR by adding small amounts of CO added to the gas mixtures either during or after the thermal cycles (Figure 6): it would appear that Pt segregation is also aided by H₂, but this conclusion is not definitive because of the possible interference of the CO probe molecule.

Finally, the behavior of the CuPt_{0.2}/SBA-15 catalyst under CO and He atmospheres was also investigating *in situ* by XAS. The near-edge region (XANES) of the spectra attests to the metallic and dispersed nature of the Pt atoms, and an electronic structure not significantly

affected by the presence of gases or temperature (Figure 7). On the other hand, analysis of the extended structure (EXAFS; Figure 8) highlights a significant change in the coordination sphere around the Pt atoms upon heating of the catalyst. Specifically, the coordination numbers for neighboring Cu and Pt atoms switch from approximately Pt-Cu to Pt-Pt coordination number ratio of 6:6 at 445 K or below to 8:4 at 495 K (Figure 9), indicating better intermetallic mixing at high temperatures and possibly additional Pt segregation to the surface, consistent with the IR results. Interestingly, the same behavior was seen with both CO and He, suggesting that the strong binding of CO to Pt may not be the main driving force justifying the diffusion reported here. It should be indicated that the segregation of Pt atoms in between the bulk and surface of the bimetallic NPs with high-Pt-content catalysts is not easy to isolate because of the presence of some Pt atoms on the surface even at low temperatures. For that, work with more diluted SAAs is desirable. We are in the process of performing *in situ* IR and XAS experiments like those reported here with more diluted alloys.

Data Availability Statement

The data that support the findings of this study are available from the corresponding author upon reasonable request.

Acknowledgements

Financial support for the work of FZ was provided by a grant from the U.S. National Science Foundation, Division of Chemistry (NSF-CHE1953843). The authors thank the beamline scientist E. Stavitski at the 8-ID beamline of the NSLS-II for support during the beamline experiments. AIF acknowledges support by a grant from the U.S. National Science Foundation, Division of Chemistry (NSF-CHE2203858). This research used the 8-ID (ISS) beamline of the National Synchrotron Light Source, a U.S. DOE Office of Science User Facilities operated for the DOE Office of Science by Brookhaven National Laboratory (BNL) under Contract No. DE-SC0012704.

References

- ¹ G. C. Bond, *Metal-Catalysed Reactions of Hydrocarbons* (Springer, New York, 2005), Fundamental and Applied Catalysis,
- ² D. Sanfilippo, and P. N. Rylander, in *Ullmann's Encyclopedia of Industrial Chemistry* (Wiley VCH Verlag GmbH & Co. KGaA, Weinheim, 2012), pp. 451.
- Z. Ma, and F. Zaera, in *Encyclopedia of Inorganic and Bioinorganic Chemistry*, edited by R.
 A. Scott (John Wiley & Sons, Ltd, Chichester, 2014), p. eibc0079.
- ⁴ J. H. Sinfelt, *Bimetallic Catalysts: Discoveries, Concepts and Applications* (John Wiley and Sons, New York, 1983),
- ⁵ R. Ferrando, J. Jellinek, and R. L. Johnston, Chem. Rev. **108** (2008) 845.
- ⁶ W. Yu, M. D. Porosoff, and J. G. Chen, Chem. Rev. **112** (2012) 5780.
- ⁷ J. A. Rodriguez, Surf. Sci. Rep. **24** (1996) 223.

- ⁸ Y. Wang, and P. B. Balbuena, J. Phys. Chem. B **109** (2005) 18902.
- ⁹ A. J. Medford *et al.*, J. Catal. **328** (2015) 36.
- ¹⁰ M. T. Greiner *et al.*, Nat. Chem. **10** (2018) 1008.
- ¹¹ V. Ponec, Appl. Catal. A **222** (2001) 31.
- ¹² P. Liu, and J. K. Nørskov, Phys. Chem. Chem. Phys. **3** (2001) 3814.
- ¹³ F. Gao, and D. W. Goodman, Chem. Soc. Rev. **41** (2012) 8009.
- ¹⁴ S. Sarfraz et al., ACS Catal. **6** (2016) 2842.
- ¹⁵ P. N. Duchesne *et al.*, Nat. Mater. **17** (2018) 1033.
- ¹⁶ J. Han et al., Chin. J. Chem. **37** (2019) 977.
- ¹⁷ R. T. Hannagan *et al.*, Chem. Rev. **120** (2020) 12044.
- ¹⁸ F. Zaera, Chem. Rev. **122** (2022) 8594.
- ¹⁹ M. Johansson, O. Lytken, and I. Chorkendorff, J. Chem. Phys. **128** (2008) 034706.
- ²⁰ L. Álvarez-Falcón et al., Surf. Sci. **646** (2016) 221.
- ²¹ B. Chen, and F. Zaera, J. Phys. Chem. C **125** (2021) 14709.
- ²² C. P. O'Brien et al., J. Phys. Chem. C **115** (2011) 24221.
- ²³ G. Gumuslu *et al.*, ACS Catal. **5** (2015) 3137.
- ²⁴ M. Luneau *et al.*, Chem. Rev. **120** (2020) 12834.
- ²⁵ E. C. H. Sykes, and P. Christopher, Current Opinion in Chemical Engineering **29** (2020) 67.
- ²⁶ M. B. Boucher *et al.*, Phys. Chem. Chem. Phys. **15** (2013) 12187.
- ²⁷ F. R. Lucci et al., Nat. Commun. 6 (2015) 8550.
- ²⁸ G. X. Pei et al., ACS Catal. 7 (2017) 1491.
- ²⁹ M. Luneau *et al.*, ACS Catal. (2019) 441.
- $^{30}\,$ Y. Cao et al., ACS Catal. 9 (2019) 9150.

- ³¹ Y. Cao et al., ACS Catal. **10** (2020) 3431.
- ³² F. R. Lucci et al., J. Phys. Chem. C **119** (2015) 24351.
- ³³ M. T. Darby *et al.*, J. Phys. Chem. Lett. **9** (2018) 5636.
- ³⁴ G. Giannakakis, M. Flytzani-Stephanopoulos, and E. C. H. Sykes, Acc. Chem. Res. **52** (2019) 237.
- ³⁵ M. T. Darby *et al.*, ACS Catal. **8** (2018) 5038.
- ³⁶ H. Thirumalai, and J. R. Kitchin, Top. Catal. **61** (2018) 462.
- ³⁷ J. Schumann *et al.*, J. Phys. Chem. Lett. **12** (2021) 10060.
- ³⁸ S. Zafeiratos, S. Piccinin, and D. Teschner, Catal. Sci. Technol. **2** (2012) 1787.
- ³⁹ J. P. Simonovis *et al.*, J. Phys. Chem. C **122** (2018) 4488.
- ⁴⁰ K. G. Papanikolaou, M. T. Darby, and M. Stamatakis, J. Phys. Chem. C **123** (2019) 9128.
- ⁴¹ S. Liu et al., ACS Catal. 9 (2019) 5011.
- ⁴² M. A. van Spronsen *et al.*, J. Phys. Chem. C **123** (2019) 8312.
- ⁴³ J. P. Simonovis *et al.*, Surf. Sci. **679** (2019) 207.
- ⁴⁴ F. Tao *et al.*, Science **322** (2008) 932.
- ⁴⁵ Z. Konuspayeva et al., Journal of Materials Chemistry A 5 (2017) 17360.
- ⁴⁶ E. V. Carino, and R. M. Crooks, Langmuir **27** (2011) 4227.
- ⁴⁷ H. Tiznado, S. Fuentes, and F. Zaera, Langmuir **20** (2004) 10490.
- ⁴⁸ F. Zaera, ChemCatChem **4** (2012) 1525.
- ⁴⁹ P. J. Chupas *et al.*, J. Appl. Crystallogr. **41** (2008) 822.
- ⁵⁰ M. A. Kohler *et al.*, J. Catal. **117** (1989) 188.
- ⁵¹ A. Dandekar, and M. A. Vannice, J. Catal. **178** (1998) 621.
- ⁵² K. Hadjiivanov, and H. Knözinger, Phys. Chem. Chem. Phys. **3** (2001) 1132.

- ⁵³ D. J. Stacchiola, Acc. Chem. Res. **48** (2015) 2151.
- ⁵⁴ N. D. Nielsen *et al.*, Surf. Sci. **703** (2021) 121725.
- ⁵⁵ T. Han *et al.*, J. Phys. Chem. C **126** (2022) 3078.
- ⁵⁶ R. A. Shigeishi, and D. A. King, Surf. Sci. **58** (1976) 379.
- ⁵⁷ R. Martin, P. Gardner, and A. M. Bradshaw, Surf. Sci. **342** (1995) 69.
- ⁵⁸ F. Zaera, J. Liu, and M. Xu, J. Chem. Phys. **106** (1997) 4204.
- ⁵⁹ M. J. Kappers, and J. H. van der Maas, Catal. Lett. **10** (1991) 365.
- ⁶⁰ J. Liu et al., J. Am. Chem. Soc. **138** (2016) 6396.
- ⁶¹ J. Finzel, and P. Christopher, Top. Catal. (2022) DOI: 10.1007/s11244.
- 62 C. T. Campbell et al., Surf. Sci. 107 (1981) 207.
- ⁶³ J. L. Gland, and E. B. Kollin, J. Chem. Phys. **78** (1983) 963.
- ⁶⁴ B. Tränkenschuh *et al.*, Surf. Sci. **601** (2007) 1108.
- 65 B. E. Hayden, and A. M. Bradshaw, Surf. Sci. 125 (1983) 787.
- ⁶⁶ B. E. Hayden *et al.*, Surf. Sci. **149** (1985) 394.
- ⁶⁷ J. A. Rodriguez, C. M. Truong, and D. W. Goodman, J. Chem. Phys. **96** (1992) 7814.
- ⁶⁸ A. M. Baró, H. Ibach, and H. D. Bruchmann, Surf. Sci. **88** (1979) 384.
- 69 Ş. C. Bădescu *et al.*, Phys. Rev. Lett. **88** (2002) 136101.
- ⁷⁰ H. Asada *et al.*, J. Chem. Phys. **63** (1975) 4078.
- ⁷¹ A. J. Renouprez, and H. Jobic, J. Catal. **113** (1988) 509.
- ⁷² S. F. Parker *et al.*, Chem. Eur. J. **25** (2019) 6496.
- ⁷³ G. Meitzner *et al.*, J. Chem. Phys. **83** (1985) 353.
- ⁷⁴ R. S. Irani, and R. W. Cahn, Nature **226** (1970) 1045.
- ⁷⁵ T. Abe, B. Sundman, and H. Onodera, Journal of Phase Equilibria and Diffusion **27** (2006) 5.

- ⁷⁶ Y. Liu, L. Zhang, and D. Yu, Journal of Phase Equilibria and Diffusion **30** (2009) 136.
- ⁷⁷ J. Tang *et al.*, J. Phys. Chem. C **119** (2015) 21515.
- ⁷⁸ L. Vega *et al.*, Materials Advances **2** (2021) 6589.
- ⁷⁹ A. J. Therrien *et al.*, Nat. Catal. **1** (2018) 192.